JOURNAL OF GUIDANCE, CONTROL, AND DYNAMICS
Vol. 31, No. 3, May–June 2008

Engineering Notes

ENGINEERING NOTES are short manuscripts describing new developments or important results of a preliminary nature. These Notes should not exceed 2500 words (where a figure or table counts as 200 words). Following informal review by the Editors, they may be published within a few months of the date of receipt. Style requirements are the same as for regular contributions (see inside back cover).

Nonlinear Control and Estimation of a Tethered Kite in Changing Wind Conditions

Paul Williams,* Bas Lansdorp,† and Wubbo Ockels‡
Delft University of Technology,
2600 GB Delft, The Netherlands

DOI: 10.2514/1.31604

I. Introduction

KITE systems have been identified as a potential means for generating power from high-altitude winds [1–3]. Many early concepts for extracting wind energy from high altitudes focused on placing a generator in the prevalent winds [4,5]. This has the major drawback of wasting a significant amount of power just to maintain the system at the desired altitude. Alternatively, keeping the generator on the ground and using a light lifting body to generate tension in the cable allows converting the wind energy into mechanical work. This line of thinking has stimulated a lot of interest in tethered kites because of the relative ease with which different concepts can be tested.

There are currently two major design concepts that have been suggested for power generation based on mechanical transmission of the wind energy: 1) horizontal-axis generators that are driven by alternating the cable length and 2) vertical-axis generators that are driven by a torque created by the tether tension. The first concept controls the motion of the lifting body in such a way that high tension is created during payout of the cable and low tension is generated during the reel-in phase. The difference in tension allows net power to be generated. The vertical-axis concept requires flying the kite in a way that maximizes the torque on the generator. Both of these concepts require that the kite can be controlled to fly suitable trajectories.

To make power generation through kites a reality, it is necessary to implement a control system that can autonomously control the kite system in a robust manner. Currently, research in this area is limited by the unavailability of sufficient data to allow accurate kite models to be constructed. Recent work has focused on the extraction of experimental data to help model identification and model development [6]. In [7], a multiplate representation of the kite was used that allowed for control by movement of the tether attachment points on the kite. However, the high flexibility of most kite systems makes modeling a challenge when viewed from a control engineer's perspective. Highly detailed models can be developed using fluid–structure interaction methodologies, but these would be too slow to enable control system development. This work builds on the work presented in [3], which details the design of nonlinear optimal power-generating trajectories for kite systems.

This paper is aimed at developing a preliminary control system for manipulating the trajectory of a tethered kite. We employ a very simple approximation of the kite dynamics by considering only the forces generated by the system. The goal is to create a means for stabilizing the kite motion around a particular set of reference trajectories under varying wind conditions. In a practical system, the wind speed is not known in general, and it fluctuates in both magnitude and direction. The control system must be capable of handling changes in wind speed and direction. In this Note, we describe the development of a nonlinear feedback controller that stabilizes the kite motion using a set of noisy measurements of the system. Numerical simulations are used to demonstrate the effectiveness of the controller for tracking power-generation trajectories. This work shows that the loop can be closed with the kite using inexact feedback and nonlinear optimal control with a representative tether dynamic model.

II. Tethered Kite Dynamic Model

Modeling of tethered systems can take on a variety of complexity, depending on the level of fidelity required. Figure 1 demonstrates different broad levels of model fidelity compared with the true system. In this Note, two separate models are used. For feedback control and nominal trajectory design, a model that treats the tether as a straight rigid body with uniform mass and distributed drag is employed. The tether is connected to the kite at one end and to a winch at the other end. The winch is used to change the cable length. The tip of the tether is represented by spherical coordinates relative to the winch, which is located at the origin of an inertial coordinate system, as shown in Fig. 1. The definition of the tether angles is such that the in-plane angle represents the position of the kite downwind, whereas the out-of-plane angle represents the crosswind drift of the kite. In the nominal trajectory design, the wind direction is assumed to be parallel to the x axis. For simulation of the true system, a more detailed model is used that represents the effects of tether flexibility. The tether is discretized into a series of point masses connected via inelastic elements. Each point mass is acted on by aerodynamic drag, gravity, and tension forces. The model uses relative spherical coordinates for an efficient representation of the equations of motion. Details on the modeling may be found in [8].

The kite is modeled as a point mass, acted on by lift and drag forces, which are generated as functions of angle of attack and roll. Because the kite attitude dynamics are not modeled, we use the angle of attack and roll angle as pseudocontrol inputs, which the real system would need to be able to track. The validity of this assumption depends on the availability of accurate models that can be used to represent the kite. For the purposes of this work, however, we assume some aerodynamic characteristics of the kite, which can later be modified to accommodate the characteristics of a particular system being studied. The kite is assumed to have a mass $\bar{m}_k$, and the tether is assumed to have a line density of ρ_c. The tether length L is used as an

Received 14 April 2007; revision received 2 September 2007; accepted for publication 3 September 2007.

*Visiting Scholar, Unit 1, 4 Maylands Avenue, Balwyn North Victoria 3104; tethered.systems@gmail.com. Member AIAA.

†Ph.D. Researcher, Faculty of Aerospace Engineering, Postbus 5058; b.lansdorp@tudelft.nl.

‡Aerospace Sustainable Engineering and Technology (ASSET) Chairholder, Faculty of Aerospace Engineering, Postbus 5058; w.j.ockels@tudelft.nl.

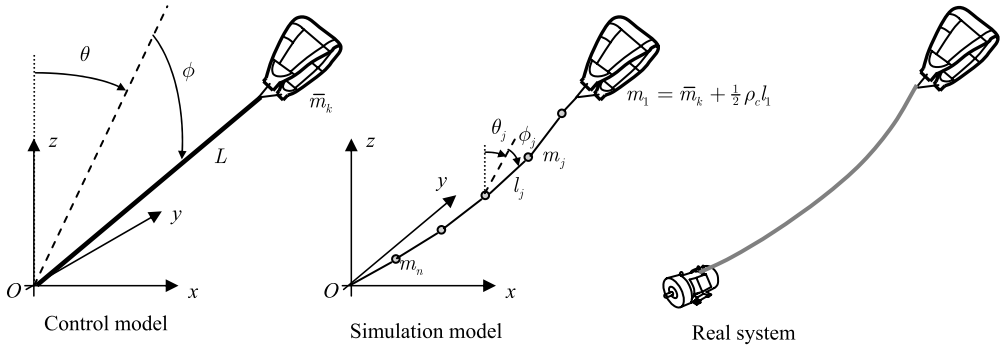

Fig. 1 Representations of a tethered kite system.

approximation for the distance to the kite from the winch. In reality, the tether takes on some curvature due to drag and gravity forces. The amount of curvature depends on the ratio of the prevailing lift forces on the kite to the mass density of the tether. For maximum power-generating trajectories, the tether tension alternates between low and high values [3], making the straight-tether assumption less realistic. The modeling error needs to be compensated by proper feedback.

The equations of motion for the simplified system are given by [3]

$$(\bar{m}_k + \tfrac{1}{3}\rho_c L)L^2\ddot{\theta}\cos^2\phi + 2(\bar{m}_k + \tfrac{1}{2}\rho_c L)L\dot{L}\,\dot{\theta}\cos^2\phi - 2(\bar{m}_k + \tfrac{1}{3}\rho_c L)L^2\dot{\theta}\dot{\phi}\sin\phi\cos\phi - (\bar{m}_k + \tfrac{1}{2}\rho_c L)gL\cos\phi\sin\theta = Q_\theta^k + Q_\theta^t \tag{1}$$

$$(\bar{m}_k + \tfrac{1}{3}\rho_c L)L^2\ddot{\phi} + 2(\bar{m}_k + \tfrac{1}{2}\rho_c L)L\dot{L}\,\dot{\phi} + (\bar{m}_k + \tfrac{1}{3}\rho_c L)L^2\dot{\theta}^2\sin\phi\cos\phi - (\bar{m}_k + \tfrac{1}{2}\rho_c L)gL\sin\phi\cos\theta = Q_\phi^k + Q_\phi^t \tag{2}$$

$$(\bar{m}_k + \rho_c L)\ddot{L} + \tfrac{1}{2}\rho_c\dot{L}^2 - (\bar{m}_k + \tfrac{1}{2}\rho_c L)L\dot{\phi}^2 - (\bar{m}_k + \tfrac{1}{2}\rho_c L)L\dot{\theta}^2\cos^2\phi + (\bar{m}_k + \rho_c L)g\cos\phi\cos\theta = Q_L^k - T \tag{3}$$

where T is the tether tension, and the superscripts k and t represent the generalized forces due to the kite and tether, respectively. The lift and drag forces due to the kite are derived using a velocity coordinate system as functions of the kite angle of attack and roll angle. It is also assumed that the yaw angle of the kite is always pointing in the relative wind direction. Hence, forces due to sideslip are not modeled. The derivation of kite and tether forces are given in [3]. The aerodynamic forces are modeled only in a simplified form. The effects of kite attitude dynamics and flexibility, as well as vortex-shedding from the tether, are potentially very important. These will need to be included in more detailed simulations of the system. It should be noted that the roll angle of the kite is defined relative to the local tether direction, rather than an inertial direction. The advantage of this definition of roll angle is that it is invariant with respect to changes in the mean wind direction.

III. Estimation and Control Architecture

To control the motion of the kite, it is necessary to be able to estimate the wind speed and direction. This is extremely important because in practice the wind can change direction and magnitude substantially over time. Furthermore, it is the wind speed at the kite that is most important, not the wind speed at the ground. Kite control begins with a set of predetermined reference trajectories that are uploaded to the flight computer, which are used to perform tracking control. In brief, the tracking controller implements a nonlinear predictive control algorithm for minimizing the deviation of the kite trajectory from the reference. This produces the set of control inputs $\boldsymbol{u}(t)$ to the real system. This in turn produces the true system state $\boldsymbol{x}(t)$, which is unknown in practice and is also a function of process noise $\boldsymbol{v}$. Using appropriate sensors, the kite system produces measurements of its motion $\boldsymbol{y}(t)$, which are subject to measurement noise $\boldsymbol{w}$. The measurements are used to produce estimates of the system state vector, wind speed, and wind direction.

A. Reference-Trajectory Generation

The reference trajectories are determined offline as a function of wind speed. These are determined so as to maximize a weighted combination of average power generated per cycle, as well as to minimize the kite pseudocontrol inputs. The pseudocontrol inputs are taken as the time derivative of angle of attack $\dot{\alpha}$ and roll angle $\dot{\varphi}$. The reference trajectories are defined to be periodic, so that for steady operating conditions the kite motion can be continually repeated to generate maximum average power per cycle. The result is a set of optimal trajectories versus wind speed in the local wind reference frame. The local wind reference frame is defined such that the x' axis is always pointing in the direction of the wind. In other words, the wind reference frame coincides with the inertial frame defined in Fig. 1 for nominal wind conditions. Details of maximum power trajectories are available in [3]. The cost function to be minimized over the cycle period T_p is given by

$$J_{\text{ref}} = \int_0^{T_p}\left[-\frac{T\dot{L}}{T_p} + (W_1\dot{\alpha}^2 + W_2\dot{\varphi}^2 + W_3\ddot{L}^2)\right]\mathrm{d}t \tag{4}$$

which is subject to the dynamic constraints given by Eqs. (1–3), as well as a set of periodicity conditions for all states and controls:

$$\boldsymbol{x}(0) = \boldsymbol{x}(T_p), \qquad \boldsymbol{u}(0) = \boldsymbol{u}(T_p) \tag{5}$$

In addition, a minimum tension constraint of 10 N is enforced on the optimal trajectories to prevent compression in the tether. The kite control parameters are constrained by the following constraints:

$$|\alpha| \le 10\ \text{deg}, \quad |\varphi| \le 30\ \text{deg}, \quad |\dot{\alpha}| \le 5\ \text{deg/s}, \quad |\dot{\varphi}| \le 5\ \text{deg/s} \tag{6}$$

The following additional constraints are imposed on the reeling:

$$\left|\frac{\Delta L}{L_{\text{ref}}}\right| \le 0.3, \qquad |\dot{L}| \le 10\ \text{m/s}, \qquad |\ddot{L}| \le 3\ \text{m/s}^2 \tag{7}$$

To prevent the kite from impacting the ground, the following constraints are also enforced:

$$|\theta| \le 80\ \text{deg}, \qquad |\phi| \le 70\ \text{deg} \tag{8}$$

The resulting nonlinear optimal control problem is discretized via the Legendre pseudospectral method [9,10]. This particular discretization is also used in the online tracking control component.

B. Nonlinear Tracking Control

The tracking controller uses the set of reference trajectories determined offline for tracking. Assuming that a wind speed estimate $W_{x'}$ is available from the online state estimator (see Sec. III.C), it is averaged over the last t_{avg} seconds (i.e., $t - t_{\text{avg}}, \ldots, t$) to produce a mean wind speed estimate $\bar{W}_{x'}$. If the current wind speed estimate

exceeds the mean estimate by a specified threshold ($|W_{x'} - \bar{W}_{x'}| > W_x^{\text{threshold}}$), then the wind speed estimate that is used for tracking is updated to the current value. This is done to prevent the reference trajectory continually changing unless there is a large enough change in the wind. By tuning the parameter $W_x^{\text{threshold}}$, we are able to reject turbulence from altering the commanded trajectory in the outer loop. The wind speed estimate is used to perform a bounded multidimensional interpolation of the reference trajectories.

Interpolating the reference trajectories as a function of wind speed assumes that the wind remains parallel to the x axis. Because in practice the wind can come from any direction, the commanded trajectory must undergo a nonlinear transformation to produce a commanded trajectory in inertial coordinates. The transformation is achieved by first converting the interpolated reference trajectory to Cartesian components of position and velocity:

$$x_t' = L' \sin\theta' \cos\phi', \qquad y_t' = L' \sin\phi', \qquad z_t' = L' \cos\theta' \cos\phi' \tag{9}$$

$$\begin{aligned} \dot{x}_t' &= \dot{L}' \cos\phi' \sin\theta' - L'\dot{\phi}' \sin\phi' \sin\theta' + L'\dot{\theta}' \cos\phi' \cos\theta' \\ \dot{y}_t' &= \dot{L}' \sin\phi' + L'\dot{\phi}' \cos\phi' \\ \dot{z}_t' &= \dot{L}' \cos\phi' \cos\theta' - L'\dot{\phi}' \cos\phi' \cos\theta' - L'\dot{\theta}' \cos\phi' \cos\theta' \end{aligned} \tag{10}$$

where the prime $(\,)'$ refers to the trajectory in the local wind reference frame. The inertial trajectory is obtained by rotating the local solution by the direction of the wind:

$$[x_t, y_t, z_t]^T = C(\tilde{\gamma})[x_t', y_t', z_t']^T, \qquad [\dot{x}_t, \dot{y}_t, \dot{z}_t]^T = C(\tilde{\gamma})[\dot{x}_t', \dot{y}_t', \dot{z}_t']^T \tag{11}$$

$$C(\tilde{\gamma}) = \begin{bmatrix} \cos\tilde{\gamma} & -\sin\tilde{\gamma} & 0 \\ \sin\tilde{\gamma} & \cos\tilde{\gamma} & 0 \\ 0 & 0 & 1 \end{bmatrix} \tag{12}$$

Here, we are assuming that the vertical component of wind velocity is negligible. The transformed solution is then converted back into spherical coordinates using the following inverse transformation:

$$L = L', \qquad \theta = \operatorname{atan2}(x_t', z_t'), \qquad \phi = \sin^{-1}(y_t'/L) \tag{13}$$

$$\begin{aligned} \dot{L} &= \dot{x}_t \sin\theta \cos\phi + \dot{y}_t \sin\phi + \dot{z}_t \cos\theta \cos\phi \\ \dot{\theta} &= \frac{\dot{x}_t \cos\theta}{L \cos\phi} - \frac{\dot{z}_t \sin\theta}{L \cos\phi} \\ \dot{\phi} &= -\frac{\dot{x}_t}{L} \sin\theta \sin\phi + \frac{\dot{y}_t}{L} \cos\phi - \frac{\dot{z}_t}{L} \cos\theta \sin\phi \end{aligned} \tag{14}$$

Equations (13) and (14) produce the trajectory in spherical coordinates relative to the inertial axes, which is suitable as a commanded trajectory for online tracking.

The online trajectory-tracking component is composed of two control loops. This is necessary to provide fast enough updates to ensure system stability. These loops can be considered as outer and inner loops. The outer loop generates a full constrained nonlinear trajectory using model predictive control based on the state estimate taken at the outer-loop sampling time, whereas the inner loop is updated at a faster rate and uses unconstrained linear receding horizon control to track the outer-loop commands. The control signals are clipped at their limits in this implementation of the inner loop.

1. *Outer-Loop Control Updates*

The outer loop seeks to find the state-control $\{\boldsymbol{x}_o(t), \boldsymbol{u}_o(t)\}$ pair that minimizes the cost function

$$\begin{aligned} J = \int_{t_s}^{t_s+T_h} &([\boldsymbol{x}_o(t) - \boldsymbol{x}_c(t)]^T \boldsymbol{Q} [\boldsymbol{x}_o(t) - \boldsymbol{x}_c(t)] \\ &+ [\boldsymbol{u}_o(t) - \boldsymbol{u}_c(t)]^T \boldsymbol{R} [\boldsymbol{u}_o(t) - \boldsymbol{u}_c(t)]) \mathrm{d}t \end{aligned} \tag{15}$$

where t_s is the current outer-loop sampling time, T_h is the outer-loop horizon length, $\boldsymbol{x}_c$ is the commanded trajectory, $\boldsymbol{Q}$ is the state weighting matrix, and $\boldsymbol{R}$ is the control weighting matrix. The state and control weighting matrices are used to trade trajectory-tracking performance with the deviation of the controls from the nominal. The cost function is minimized subject to the state equations defined by Eqs. (1–3), together with the initial conditions

$$\boldsymbol{x}_o(t_s) = \hat{\boldsymbol{x}}(t_s) \tag{16}$$

where $\hat{\boldsymbol{x}}(t_s)$ is the state estimate at the outer-loop sampling time. For consistency with the generated trajectories, the outer loop is also subject to a path constraint on the tether tension,

$$T \geq T_{\min} \tag{17}$$

as well as lower and upper bounds on the states and controls, as follows:

$$\boldsymbol{x}_{\min} \leq \boldsymbol{x}_o(t) \leq \boldsymbol{x}_{\max}, \qquad \boldsymbol{u}_{\min} \leq \boldsymbol{u}_o(t) \leq \boldsymbol{u}_{\max} \tag{18}$$

This optimal control problem is discretized using the Legendre pseudospectral method and is solved using the solver SNOPT [11]. The initial guess for the trajectory is always the commanded motion $\{\boldsymbol{x}_c(t), \boldsymbol{u}_c(t)\}$, which is generally a good guess for the nonlinear programming. However, to safeguard against possible failures of the solver or solutions that exceed the sampling time, the outer loop must be implemented with a local tracking controller. The local tracking controller is discussed in the following subsection.

2. *Inner Linear Receding Horizon Tracking Controller*

One of the inherent difficulties of any nonlinear predictive control algorithm is that the solution time per call is not constant, nor is it in any way predictable. This is potentially devastating to a real-time system that relies on computations taking place within a particular time. Therefore, a maximum time limit must be set (or a maximum number of iterations) so that if a solution is not obtained within the limit, a restart with a new state estimate is undertaken. Between sampling times, an inner-loop tracker is used to keep the system close to the outer-loop trajectory. This has the advantage that disturbances introduced between sampling times can be partially, or completely, rejected before a new sample. However, this will only be good for small disturbances in which the linearized system dynamics employed by the inner-loop tracker are valid. However, clearly, a 180-deg change in wind direction would be beyond the capabilities of a linear tracking controller, hence the need for the outer loop. The main advantage of the inner loop is that failure of the outer loop can be handled in the short term by the inner loop. Note, however, that too many sequential failures of the outer loop is likely to cause total failure of the tracking control architecture. A possible safeguard would be to revert the system to one of the nominal optimal trajectories contained in the lookup table. It is inevitable, however, that the system will meet certain conditions that result in failure of the tracking controller. The absence of wind is one such example.

The inner-loop tracker is implemented using a pseudospectral discretization of the linearized dynamics around the time-varying reference trajectories [12,13]. The final result is a feedback controller of the form

$$\delta\boldsymbol{u}(t) \triangleq \boldsymbol{K}(t; T_h)\delta\boldsymbol{x}(t) \tag{19}$$

where the feedback gain matrix $\boldsymbol{K}(t; T_h)$ is a function of time and the horizon length T_h.

C. Nonlinear State Estimation

To enable the implementation of the controller discussed in the previous section, full state feedback of the kite position (tether angles, tether length, and length rate), as well as the kite angle of attack and roll angle, is assumed. Although the kite position can be measured directly using GPS, for example, the velocities need to be estimated by some means. Here, we assume that the only measurements available are GPS coordinates of the kite, tension components measured at the ground winch, and tether length and

length rate. It would also be possible to use an inertial measurement unit to provide more comprehensive kite state estimates. However, for simplicity in this initial development stage, an inertial measurement unit is not used. Therefore, obtaining the full state vector of the system requires an estimator. Furthermore, the controller also requires an estimate of the wind speed and direction. Both of these are estimated by augmenting the kite state vector with additional state variables.

The kite system is nonlinear and relatively complex when the lift and drag forces of the kite and tether are taken into account. The Kalman filter is able to perform state estimation in an optimal manner for linear systems in which the probabilistic distributions for the variables are Gaussian. For nonlinear systems, the extended Kalman filter (EKF) has been the method of choice for several decades. However, the EKF uses a first-order linearization of the process model, which requires Jacobians of the process model. In addition, the linear approximations can lead to large errors in the posterior mean and covariance. The unscented Kalman filter (UKF) [14] uses a set of deterministic sampling points that are directly propagated through the process and measurement models, circumventing the need for direct linearization. Although the standard UKF performs well for the kite system, we have implemented a square-root version of the filter to improve numerical stability of the filter [15].

IV. Numerical Simulation Results

The reference trajectories are generated with the cycle period held fixed at 20 s, although it should be noted that for maximum power generation, the period should be kept as large as possible [3]. The weightings in the cost specified in Eq. (4) are selected as $W_1 = W_2 = W_3 = 5$. This provides a good compromise between power generation and smooth kite controls. The system parameters that are used in this study are provided in Table 1. The reference trajectories were generated for wind speeds between 8 and 20 m/s spaced at 1 m/s. The optimal reference trajectories are shown in Fig. 2, which illustrates that the kite moves in progressively larger trajectories as the wind speed increases. The optimal power-generation trajectories involve the kite moving in the crosswind direction to maximize the relative airspeed of the kite.

For closed-loop simulation, the initial wind speed is selected as 10 m/s with zero angle; that is, it coincides with the nominal wind conditions. The sampling time for the outer loop is 1 s, with a total simulation time of 500 s. The outer-loop horizon length is 4 s, and 16 nodes are used in the pseudospectral predictive controller to update the trajectories. The system is subject to the same constraints that were used to generate the original reference trajectories, except that the allowable angle of attack of the kite is increased to 15 deg, and the allowable tether angles are increased to $|\theta| \leq 89$ deg and $|\phi| \leq 89$ deg. Gust components are added to the mean wind with a standard deviation of 0.25 m/s. Random changes in the wind direction are also simulated with a standard deviation of 1 deg. Large random changes to the mean wind speed are incorporated every 10 s. Furthermore, the wind direction is changed every 40 s by adding a random increment to the wind direction with a standard deviation of 5 deg. After 450 s of simulation time, no large perturbations are simulated, to examine the convergence of the controller to a near steady path. The wind direction changes in a steady manner from 0 to 180 deg in a period of 65 s. The wind direction commences changing after a period of 30 s. The true trajectories are simulated using relative and absolute tolerances of 10^{-9} using a lumped-mass model of the tether discretized into 10 elements.

Table 1 Nominal system parameters

Parameter	Values
Kite and sensor mass $\bar{m}_k$	50 kg
Tether length L	2000 m
Tether density ρ_c	3.141 kg/km
Tether diameter d	2 mm
Lift curve slope C_{L_α}	4.4/rad
Zero-lift drag C_{D_0}	0.02
Lift-induced drag K	0.1
Kite wing area S	25 m^2

The inner loop is updated at 10 Hz and state estimates are generated at a rate of 100 Hz. The weighting matrices for the feedback controller are selected as

$$\boldsymbol{Q} = \text{diag}[100, 100, 100, 100, 100, 100, 100, 100] \tag{20}$$

$$\boldsymbol{R} = \text{diag}[100, 100, 100] \tag{21}$$

$$\boldsymbol{S}_f = \text{diag}[1000, 1000, 1000, 1000, 1000, 1000, 10, 10] \tag{22}$$

where the state vector is defined as $\boldsymbol{x}(t) = \{\theta, \dot{\theta}, \phi, \dot{\phi}, L, \dot{L}, \alpha, \varphi\}$, and the controls are defined as $\boldsymbol{u}(t) = \{\dot{\alpha}, \dot{\varphi}, \ddot{L}\}$. The measurement vector is defined by

$$\boldsymbol{y} = [L\sin\theta\cos\phi, L\sin\phi, L\cos\theta\cos\phi, T\sin\theta\cos\phi, T\sin\phi, T\cos\theta\cos\phi, L, \dot{L}] \tag{23}$$

which represents the inertial kite position obtained using GPS, the tension vector measured at the ground station, and length states. The measurement noise is assumed to have standard deviations of 5 m on the position error of the kite, 30 N on tension components, 0.2 m on tether length, and 0.5 m/s on length rate. These are conservative estimates of the GPS accuracy and tension-measurement accuracy of the sensors installed on the kite system [6]. The process noise covariance is selected as follows:

$$\boldsymbol{Q}_{\text{process}} = \text{diag}[10^{-6}\ \text{rad}^2, 10^{-3}\ (\text{rad/s})^2, 10^{-6}\ \text{rad}^2, 10^{-3}\ (\text{rad/s})^2, 10^{-6}\ \text{rad}^2, 0.025\ \text{m}^2, 0.25\ \text{deg}^2, 0.25\ \text{deg}^2, 25\ (\text{m/s})^2, 100\ \text{deg}^2] \tag{24}$$

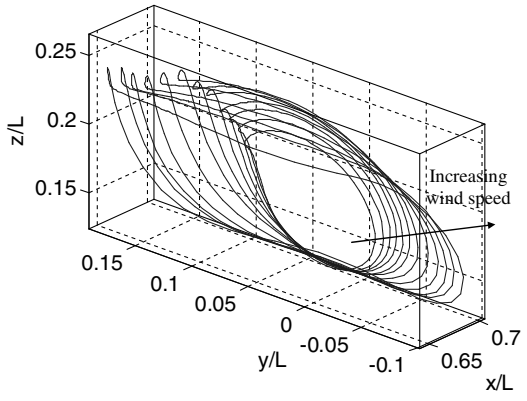

Fig. 2 Optimal periodic reference trajectories for a power-generating kite system as a function of wind speed.

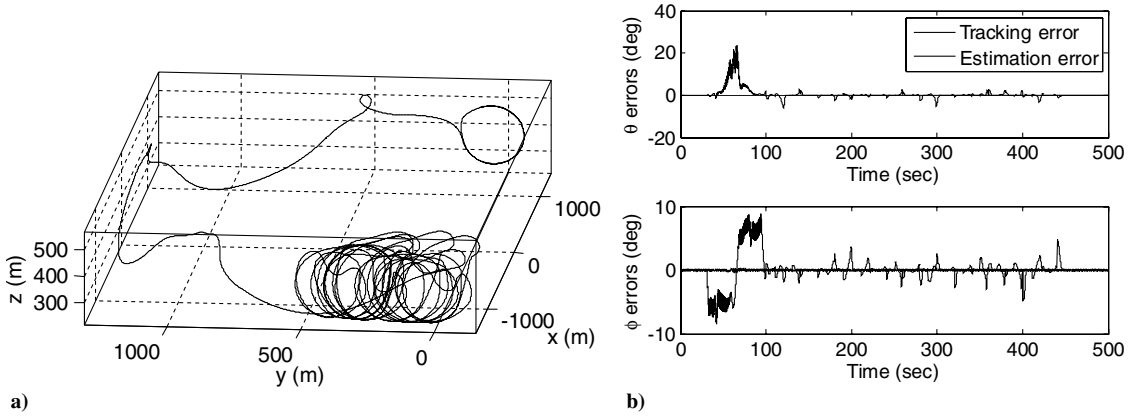

a) b)

Fig. 3 Closed-loop trajectory simulation results for linearly changing wind direction and gusts a) three-dimensional trajectory and b) angle tracking and estimation errors.

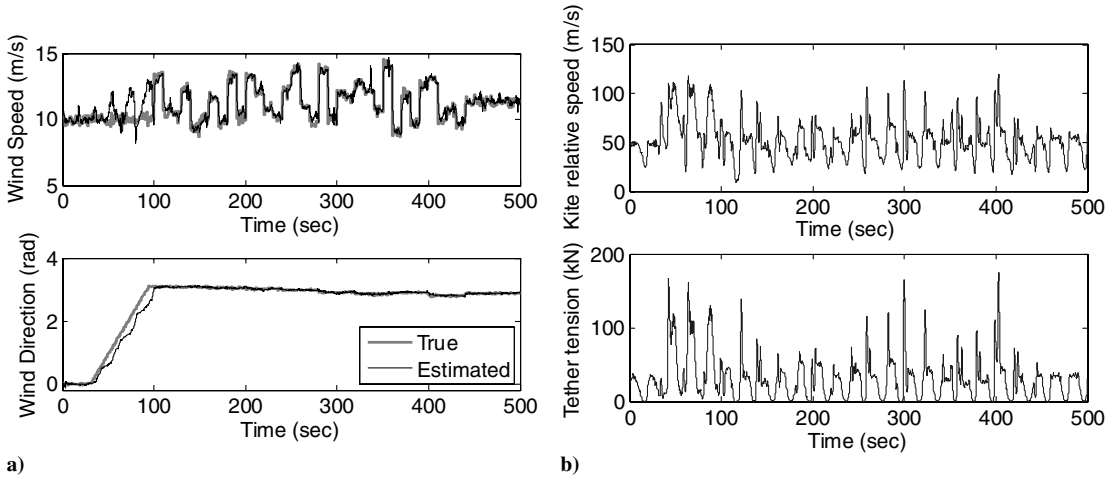

a) b)

Fig. 4 Kite closed-loop simulation results: a) simulated and estimated wind speed and direction and b) kite relative air speed and tether tension at the ground station.

where the state vector for estimation is $\boldsymbol{x}(t) = \{\theta, \dot{\theta}, \phi, \dot{\phi}, L, \dot{L}, \alpha, \varphi, \bar{W}_x, \gamma\}$. The process noise values were selected to enable changes in the wind conditions to be tracked without significant lag. Large process noise values are similarly required when tracking moving objects with constant velocity trackers, because actual noise values are difficult to determine and the Gaussian noise assumption is easily violated. It has been found that the proposed simplified tether model is a reasonably accurate representation of the tether system [3].

Example closed-loop simulation results of the kite trajectory are shown in Fig. 3. Figure 3a shows the true kite trajectory in Cartesian coordinates as it undergoes a complete change in orientation due to the shifting direction of the wind. The results illustrate good closed-loop performance for the system as it undergoes large changes in wind speed and direction. The average power generated during the simulation was approximately 31.6 kW. Figure 3b shows the control tracking errors together with the estimation errors. The initial tracking and final tracking are excellent, and there are only small fluctuations in wind speed and direction. The largest tracking errors occur as the wind rapidly changes direction. In addition, each time the mean wind speed changes, the tracking error spikes. This is due to the sudden changes in the reference trajectory. Figure 4a summarizes the wind speed and direction during the simulation. As the wind undergoes a change in direction, the direction estimate lags behind the true direction, which also induces errors in the estimated wind speed. These errors translate into errors in the estimated kite angle of attack. Errors in wind estimates lead to the use of reference trajectories that are not appropriate for the prevailing wind conditions, and hence the kite struggles to track them with high accuracy. In addition, because the wind direction is changing constantly, the controller is unable to keep up in real time, due to the lags in control action. In spite of these challenges, the system remains stable and the tracking errors are bounded. The unscented filter is very effective at estimating the kite state vector. The maximum position error due to estimation is less than 3 m, with a mean of 0.77 m.

Figure 4b illustrates important physical effects that have hitherto been ignored: namely, the kite air speed and tether tension. The kite air speed directly affects the kite lift and hence the tether tension. When there is a sudden change in wind or a change in angle of attack, there is a large peak in the relative speed of the kite. These can be up to 100 m/s for the present configuration. This is nearly twice the approximate nominal speed of 50 m/s seen at the beginning and end of the simulation. The changes in relative speed induce large peaks in the tether tension. The nominal tension oscillates between approximately 35 kN and 0 N. However, peaks of over 170 kN are recorded in the closed-loop response. These loads would easily snap a cable made using currently available materials. The authors have observed similar large tension spikes in recorded flight data for surfkites that have resulted in tether severance. However, the extreme peaks seen in these results would be relieved in reality somewhat, due to the fact that the wind does not tend to jump as rapidly as simulated here. In addition, cable elasticity and longitudinal damping can help to reduce the peak tension loads. These important effects have not been considered here and will need to be addressed in future system design. In addition, optimal design configurations capable of handling the large stresses induced by the kite need to be considered. Other factors that may improve performance are the inclusion of a

pitot tube on the kite to obtain an external source for the air data used by the controller.

V. Conclusions

A nonlinear control architecture for stabilizing the motion of a kite on time-varying reference trajectories was developed. The controller combines a nonlinear outer loop based on the Legendre pseudospectral method that adjusts the trajectories to be followed by the system in response to changes in wind speed and direction. The updated reference trajectories are tracked using an inner-loop controller based on the time-varying linearized dynamics. The controller is implemented with a nonlinear state estimator that uses an unscented Kalman filter. Numerical simulation results show that control of the kite can be achieved under changing wind conditions using filtered measurements in the feedback loop. The least accurate feedback parameters are the estimated wind conditions (speed and direction), which also induce large tracking errors. However, the overall closed-loop performance is still very good despite these uncertainties.

References

[1] Loyd, M. L., "Crosswind Kite Power," *Journal of Energy*, Vol. 4, No. 3, 1980, pp. 106–111.

[2] Ockels, W. J., "Laddermill, a Novel Concept to Exploit the Energy in the Airspace," *Aircraft Design*, Vol. 4, No. 2, 2001, pp. 81–97. doi:10.1016/S1369-8869(01)00002-7

[3] Williams, P., Lansdorp, B., and Ockels, W., "Optimal Cross-Wind Towing and Power Generation with Tethered Kites," *Journal of Guidance, Control, and Dynamics* (submitted for publication); also AIAA Paper 2007-6823.

[4] Riegler, G., Riedler, W., and Horvath, E., "Transformation of Wind Energy by a High-Altitude Power Plant," *Journal of Energy*, Vol. 7, No. 1, 1983, pp. 92–94.

[5] Fletcher, C. A. J., and Roberts, B. W., "Electricity Generation from Jet-Stream Winds," *Journal of Energy*, Vol. 3, July–Aug. 1979, pp. 241–249.

[6] Lansdorp, B., and Ockels, W., "Towards Flight Testing of Remotely Controlled Surfkites for Wind Energy Generation," AIAA Paper 2007-6643, Aug. 2007.

[7] Williams, P., Lansdorp, B., and Ockels, W., "Flexible Tethered Kite with Moveable Attachment Points, Part 1: Dynamics and Control," AIAA Paper 2007-6628, Aug. 2007.

[8] Williams, P., Lansdorp, B., and Ockels, W., "Modeling and Control of a Kite on a Variable Length Flexible Inelastic Tether," AIAA Modeling and Simulation Conference, AIAA Paper 2007-6705, Aug. 2007.

[9] Elnagar, J., Kazemi, M. A., and Razzaghi, M., "The Pseudospectral Legendre Method for Discretizing Optimal Control Problems," *IEEE Transactions on Automatic Control*, Vol. 40, No. 10, 1995, pp. 1793–1796. doi:10.1109/9.467672

[10] Ross, I. M., and Fahroo, F., "Legendre Pseudospectral Approximations of Optimal Control Problems," *Lecture Notes in Control and Information Sciences*, Vol. 295, Springer–Verlag, New York, 2003, pp. 327–342.

[11] Gill, P. E., Murray, W., and Saunders, M. A., "SNOPT: An SQP Algorithm for Large-Scale Constrained Optimization," *SIAM Journal on Optimization*, Vol. 12, No. 4, 2002, pp. 979–1006. doi:10.1137/S1052623499350013

[12] Williams, P., "Receding Horizon Control Using Gauss–Lobatto Quadrature Approximations," AAS/AIAA Astrodynamics Specialist Conference, American Astronautical Society, Paper 05-349, Aug. 2005.

[13] Yan, H., Fahroo, F., and Ross, I. M., "Real-Time Computation of Neighboring Optimal Control Laws," AIAA Paper 2002-4657, Aug. 2002.

[14] Julier, S. J., Uhlmann, J. K., and Durrant-Whyte, H., "A New Approach for Filtering Nonlinear Systems," *Proceedings of the 1995 American Control Conference*, American Automatic Control Council, Evanston, IL, 1995, pp. 1628–1632.

[15] Van der Merwe, R., and Wan, E. A., "The Square-Root Unscented Kalman Filter for State and Parameter-Estimation," *Proceedings of the 2001 IEEE International Conference on Acoustics, Speech, and Signal Processing*, Vol. 6, Inst. of Electrical and Electronics Engineers, Piscataway, NJ, May 2001, pp. 3461–3464.